Micron 159 (2022) 103294

Contents lists available at ScienceDirect

Micron

journal homepage: www.elsevier.com/locate/micron

Comparison of microscopic techniques to study the diversity of the bitumen microstructure

Johannes Mirwald [a,*,1], Bernhard Hofko [a,2], Georgios Pipintakos [b,3], Johan Blom [b,4], Hilde Soenen [c,5]

[a] Christian Doppler Laboratory for Chemo-Mechanical Analysis of Bituminous Materials, Institute of Transportation, TU Wien, Gusshausstrasse 28/E230-3, Vienna 1040, Austria
[b] EMIB research group, University of Antwerp, Groenenborgerlaan 171, Antwerp 2020, Belgium
[c] Nynas NV, Groenenborgerlaan 171, Antwerp 2020, Belgium

ARTICLE INFO

Keywords:
Bitumen
Microscopy
CLSM
AFM
OIM
Image analysis
Microstructure quantification

ABSTRACT

Bitumen characterisation and differentiation usually involve a combination of mechanical and chemical analyses. However, these methods provide limited information on the diversity caused by the binders' origin or processing method. Thus, the question arises whether the bitumen microstructure can be used to identify these issues. In this study, microscopic methods, including brightfield, darkfield and fluorescence optical inverse microscopy (OIM), as well as confocal laser scanning microscopy (CLSM) and atomic force microscopy (AFM), were used to investigate the bitumen surface. Five different binders varying in their origin and production method were selected. The results show that CLSM, AFM and OIM darkfield can adequately capture a specific surface microstructure known as the bee structure, whereas brightfield in the OIM and optical CLSM show the surrounding peri phase, which exhibits a strong fluorescence. All visbroken binders show bee structures surrounded by a pronounced peri phase. On the other hand, one of the straight distilled binders does not show any microstructure, while the second straight distilled binder displays smaller bee structures surrounded by a small peri phase. Results from the image processing evaluation reveal that the area covered by bee structures is in the range of 2.4 – 4.3% for those binders that developed a surface microstructure. These results indicate a good accordance between the three microscopic techniques selected. However, a clear differentiation between the binders is difficult to obtain. Nonetheless, this work shows how these techniques can be used to their maximum capabilities regarding the obtained microstructural information and may help solve future questions regarding ageing, modification or rejuvenation.

1. Introduction

The characterisation of bituminous materials, particularly the chemical characterisation, is a challenging task, as bitumen consists of a mixture of hydrocarbons composed of straight-chain or branched aliphatic structures, polycyclic aromatic hydrocarbons, and all possible combinations of both structural types. Additionally, a limited number of heteroatoms like oxygen, nitrogen and sulfur as well as traces of metals like nickel and vanadium are present. While conventional bitumen evaluation methods provide information on the mechanical behaviour, chemical analysis tries to explain this behaviour and link it to the molecular species present within the material. Methods like the dynamic shear rheometer (DSR) for the rheological properties and Fourier-Transform-Infrared (FTIR) spectroscopy for chemical information are commonly used to investigate binders and to evaluate essential questions related to hot topics such as ageing (Jing et al., 2019; Poulikakos

* Corresponding author.
E-mail address: Johannes.mirwald@tuwien.ac.at (J. Mirwald).
[1] Johannes Mirwald: 0000–0001-5025–7427
[2] Bernhard Hofko: 0000–0002-8329–8687
[3] Georgios Pipintakos: 0000–0002-7027–2672
[4] Johan Blom: 0000–0002-0510–8067
[5] Hilde Soenen: 0000–0002-5311–500X

https://doi.org/10.1016/j.micron.2022.103294
Received 1 April 2022; Received in revised form 5 May 2022; Accepted 8 May 2022
Available online 18 May 2022

et al., 2019). The DSR method, if tested before and after short- and long-term ageing can capture differences between various binders, but a direct link to the chemical composition is still missing. In the European standard, bituminous materials are classified according to needle penetration and softening point, but an evaluation after long-term ageing test is still not mandatory. Therefore, binders with an entirely different ageing behaviour, and linked to this a different chemical composition, may end up in the same specification class. The addition of selected chemical tests, such as FTIR spectroscopy, could be suitable to shed more light on this matter (Weigel and Stephan, 2018). However, a more complex post process spectral analysis may be needed to really uncover differences between various binders, crude oil sources and refinery procedured. Furthermore, such quantification methods need to be evaluated on an international level to ensure their universal applicability and validity. Thus, the quest for other suitable test methods to tackle this problem are sought after. A possible solution and alternative approach could be provided by the evaluation of the (surface) microstructure.

In recent years, many microscopic techniques have been employed to evaluate the bitumen microstructure. One, if not the most used technique, is atomic force microscopy (AFM). Loeber et al., (1996). were one of the first to report the appearance of bee-shaped microstructural features on the surface of bitumen using an AFM. Compared to many other microscopic techniques, this device can resolve surfaces below the Abbe diffraction limit by simply scanning or tapping the surface with a nanometre-sized tip. Thus, it has become one of the most popular techniques to investigate the bitumen microstructure and tackle the question mentioned above on the origin or reason for the microstructure (Masson et al., 2006; Aguiar-Moya et al., 2015, 2017). While, for example, Blom et al., (2021) link the appearance of the bee structures to the presence of waxes, Hofko et al., (2016) found a connection between asphaltenes and bee structures.

Environmental scanning electron microscopy (ESEM) is another technique that can overcome the Abbe limit and resolve the bitumen microstructure (Lu et al., 2018; Mikhailenko et al., 2017; Stangl et al., 2006). By doing so, researchers have observed a string-like network that becomes denser and coarser with ageing (Mikhailenko et al., 2017; Stangl et al., 2006). It is not yet clear how this network is linked to the surface microstructure found in the AFM. Current assumptions claim that the electron beam can remove the volatile parts of the material near the surface, which leaves a remaining network behind that can withstand the electron beam (Rozeveld et al., 1997).

Besides these microscopic techniques that overcome the Abbe limit, light can also be used to observe the bitumen microstructure. However, here the Abbe diffraction limit restricts the resolution of an optical image, as it is proportional to the wavelength of the light used. Due to this physical limitation light, in the wavelength range of 400 – 800 nm, cannot be used to obtain details on the nano level. Nonetheless, standard optical inverse microscopes (OIM), containing different modes such as brightfield, darkfield or fluorescence, can be utilised to look at the material from different angles or perspectives. Brightfield provides similar information compared to AFM, but at a lower resolution, as merely the material's surface is observed in reflectance. Since the material is non-transparent, an inverse setup is usually deployed. This has been used by Ramm et al. (2019), who have looked into the phenomenon of the bee structure formation in dependency of temperature. Similar work was performed by (Nahar et al., (2013), where a temperature-dependent experimental study with an AFM showed that a formation of the bee structure was observed upon cooling and a disappearance upon heating.

Ramm et al., (2016) also used another optical method, namely darkfield microscopy. This method, contrary to brightfield, only enables light from the outer region of the illumination cone to reach the sample surface at an angle of 45°. As the light is coming from such an angle, merely light scattering objects in the focal plane will change the angle of reflection of the incoming light, which is then detected by the camera. If the surface does not contain any light scattering particles, the light will leave the focal plane at the same angle of 45°, resulting in a dark image without contrast. Thus, darkfield microscopy will only work if the material or parts of the materials surface exhibit light scattering properties and will therefore illuminate these objects, while leaving non-light scattering matter in the dark. In their work, Ramm et al. have observed small light scattering particles which they called ants. However, they have found that by varying the excitation wavelength, different depths of penetration could be achieved, which resulted in an increasing amounts of light scattering particles to be detected. Mirwald et al (Mirwald et al., 2020a) have also used darkfield microscopy and compared it to fluorescence microscopy and spectroscopy. Their recordings indicated that the light scattering particles in bitumen exhibit a strong fluorescence. However, a significant difference from previous studies was detected, as the sample preparation technique involved the usage of a silicone mould and freezing of the sample, which led to an interface formation, rather than a free surface formation. Thus, these parameters might not provide the same conditions for the surface to relax naturally or reach equilibrium, as no bee structures or similar features were found.

Similar results were found by samples captured with a confocal laser scanning microscope (CLSM). In these studies, the devices required the sample to be covered with a cover slide, which means that not the sample surface but an interface between glass and bitumen has been investigated (Bearsley et al., 2004; Handle et al., 2016; Lu et al., 2005). While all of these studies tried to uncover the microstructure involved, they have all found varying reasons indicating towards waxes or asphaltenes as the origin of the microstructure. Recent work by Blom et al., (2021) used a new confocal microscope that enables the possibility to measure at the sample surface, compared to the previous interface measurements.

While the possibility of recording the bitumen microstructure has helped the community a lot in terms of understanding and partially differentiating bitumen, its actual implementation and quantification remains a difficult task. Up to now, these images were mainly used to either prove the existence of various hypotheses in regards to the bitumen model and composition or simply show a link between rheology, chemistry and morphology. However, a comprehensive quantification or differentiation of various types of bitumen, ageing states or modifications has not been addressed often. For example, Hasheminejad et al., (2021) have tackled this question and applied a deep learning process to process differential interference contrast images captured with a CLSM. This process involved using an image labeller application of MATLAB, a pre-processing in the software from the attached confocal microscope (Keyence VK-Multi File Analyser), and the final trained algorithm (based on a neural network) to detect all bee structures at the surface. Another, less sophisticated approach was conducted by Mirwald et al., (2020a); (2020b), who used the particle analysis toolkit in an imaging process software (ImageJ Fiji) to quantify fluorescence and darkfield microscopic images. The processes involved subtracting a background in the microscope software (Nikon Elements BR) followed by a subsequent default threshold definition and particle analysis in the software, which yields the particle number and area. This threshold definition is the most crucial and difficult task in such an imaging analysis, as it basically determines the outcome of your result and needs to be adjusted in dependency of the binder. In a similar study by Pipintakos et al., (2021a), quantification of the bee structure metrics was succeeded for AFM and CLSM images before and after ageing and showed that the two techniques were in good agreement for the bee percentage and normalised area of the bees. At the same time, differences were observed for the waveform characteristics and the probabilistic shape values of the structures. In this study height thresholds for the peak and valleys of the bee structures were imposed for the AFM images after removing any curvature effects of the background (using the Gwyddion software). Similar height thresholds were determined for the CLSM images (Keyence VK-Multi File Analyser). Albeit previous

literature has shown the potential of microscopic image processing, a thorough comparison between all the existing microscopes for bitumen applications is yet to be performed.

In this study, two laboratories worked together to investigate the surface microstructure of various binders using three microscopic techniques. An initial comparison to FTIR spectra highlights potential future advantages of microscopy. Then, the OIM in three different working modes: brightfield, darkfield and fluorescence, which the first laboratory conducted, will be compared to the images recorded with the CLSM and AFM from the second laboratory. Based on previous tests conducted with an AFM, a variety of binders displaying different surface morphologies was selected. These binders included straight distilled binders form various origins as well as several visbroken binders. Furthermore, the respective laboratories performed two different particle or microstructure evaluation procedures. Subsequent comparison will reveal whether the received images from these three microscopic techniques can be linked and how the particle analysis or microstructure evaluation can be used to quantify the microstructure. The gathered knowledge should act as a basis for what one can expect when performing microscopy with these techniques and how various binders may differ depending on the origin and/or the processing method.

2. Materials and methods

2.1. Materials

In this study, five unmodified bituminous binders were investigated. In order to highlight the diversity of the bitumen microstructure, straight distilled (A and B) and visbroken (C, D and E) binders were included. Further details can be found in Table 1.

2.2. Sample preparation

Since this study was conducted in two different laboratories, a consistent sample preparation routine was followed, adopting the sample preparation elaborated in Pipintakos et al., (2021b). This involved the following steps: 5 g of the respective binder was cut out from below the surface of a large bitumen container using a heated spoon and was transferred into a metal can. The can was covered with a lid and placed in a preheated oven set to 150 °C. After 5 min of heating, which induces little to no oxidation, the liquid binder was homogenised using a thermometer. Three droplets were applied onto the three cavities of the microscopic slide (for microscopy) and four droplets on four slips of silicone paper (for FTIR spectroscopy). While the FTIR spectroscopy samples were directly placed in a crystallisation dish and covered with a metal lid, the microscopy slides were placed on a preheated heating plate set to 150 °C for 1 min. This allowed the binder droplets to spread and form a thin, flat film. After removing the slide from the heating plate, it was also placed in the same crystallisation dish and covered with a metal lid. While samples for spectroscopy were measured within 1 h after preparation, the samples for microscopy were covered with a metal lid (to prevent dust contamination) and stored at room temperature in a dark, climatised room for 24 h. The resting time for spectroscopy and microscopy tests were selected based on previous experiences and literature (Blom et al., 2021; Nahar et al., 2013; Mirwald et al., 2022a). It is yet uncertain whether the entire resting time of 24 h is needed for the microstructure to develop. However, as this work focused on the observations made with different microscopes, a detailed resting time study would exceed the content of this study.

Table 1
Information and properties of all five binders.

Binder	Refinery Process	Paving Grade	Softening Point [°C]	Penetration at 25 °C [0.1 mm]
A	Straight distilled (waxy crude)	50/70	51.3	42
B	Straight distilled (wax-free crude)	50/70	47.7	64
C	Visbroken	50/70	49.8	52
D	Visbroken	50/70	46.8	67
E	Visbroken	160/220	39.2	190

2.3. Methods

2.3.1. FTIR spectroscopy

A Bruker Alpha II FTIR spectrometer was used to record the FTIR spectra. The device is equipped with a Deuterated Triglycine Sulfate (DTGS) detector and an attenuated total reflection (ATR) unit that contains a diamond crystal. The spectra were recorded in absorbance within a wavenumber range of 4000 – 680 cm^{-1}, a resolution of 4 cm^{-1} and 24 scans. A background spectrum of the empty, clean ATR crystal was recorded prior to each measurement. The binder specimen was applied to the ATR crystal within 1 min after recording the background. Each specimen was scanned with four repetitions, resulting in four spectra per specimen. As four specimens per binder were prepared, 16 spectra were recorded per binder.

The resulting spectra were processed in the attached software OPUS. Here, all 16 spectra for each binder were normalised using a min-max normalisation in the range of 3,200 – 2,800 cm^{-1}, setting the aliphatic signal at 2,920 cm^{-1} at a numerical maximum of 2 and the minimum of 0 around 3100 cm^{-1}. This normalisation provided a good reflection of the raw data and was recommended by the supplier, as it reduces the error coming from the diamond crystal which usually exhibits the lowest intensity in a spectrum. The normalised data was full baseline integrated in the following ranges:

- Carbonyls (AI_{CO}): 1,660 – 1,800 cm^{-1}
- Sulfoxides (AI_{SO}): 1,079 – 984 cm^{-1}
- Reference aliphatic band (AI_{CH3}): 1,525 – 1,350 cm^{-1}

The obtained values from the 16 spectra were used to calculate the ageing index (AI_{FTIR}) according to Eq. (1) and were statistically evaluated by mean values and standard deviation (Mirwald et al., 2022a). Together with a specific selection of spectra, these ageing indices will be shown in the result section.

$$AI_{FTIR} = \frac{AI_{CO} + AI_{SO}}{AI_{CH_3}} \quad (1)$$

2.3.2. Optical Inverse Bright-, Darkfield and Fluorescence Microscope (OIM)

A Nikon Optical Inverse bright-, darkfield and fluorescence microscope (OIM) was one of the three microscopic setups used to capture the microstructures of the binders. To highlight the differences in the working modes, a schematic drawing is displayed in Fig. 1.

The setup consists of an industrial flexible column stand, a motorised Märzhäuser stage (X, Y, Z), an 100x CFI TU Plan objective (BD 100x, N. A. 0.80, W.D., 4.5 mm), a Nikon DS-Fi3 camera, an epi fluorescence unit and a pE-4000-Universal LED as the light source, which contains 15 different LEDs ranging from 365 to 770 nm. For the bright- and darkfield images the 500 nm LED was selected, as this LED has the least effect on possible oxidation reactions while still providing sufficient contrast-to-illumination ratio (Mirwald et al., 2022b). The epi unit contains three different filter blocks for brightfield, darkfield and fluorescence respectively. The brightfield images were recorded with an exposure time of 5 ms, while darkfield images were captured after an exposure time of 500 ms. The difference between the two settings can be explained by the differences in their basic principle (see Fig. 1). The bright field filter-block and objective do not block any light from the light source. However, the darkfield filter-block and objective block light in the centre of the illumination cone, only letting light from the outer region reach the sample surface at a 45° angle. If nothing in the

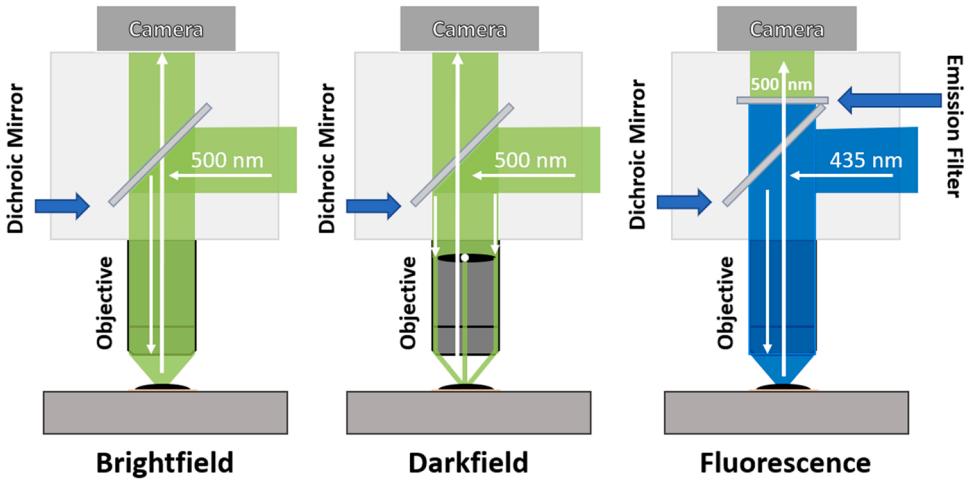

Fig. 1. Schematic overview of the OIM modes: Brightfield (left), darkfield (middle) and fluorescence (right).

surface or subsurface of the material is scattering light, no information is collected by the camera. Thus, a dark image is obtained. However, if the sample contains any light scattering particles near the surface, the incoming light will be scattered and changes its angle of reflection. This light with an altered angle of reflection travels through a dichroic mirror and is detected by the camera. Since the overall amount of light in darkfield is much less than in brightfield, a higher illumination time is required to obtain sufficient contrast. A custom-made filter was used for the fluorescence mode, which contains the following filters: An excitation filter at 403/95 nm (353–452 nm), an emission filter (long pass) at 500 nm, and a dichroic mirror at 495 nm. Since the fluorescence of the bitumen is much lower than the reflection in the brightfield mode, an exposure time of 900 ms was selected.

All images were recorded in the attached software NIS elements BR. Since the sample surfaces are not entirely plane, a z-stacking tool was used in the range of ± 10 micrometres around the focal plane of the binder specimen, followed by a subsequent z-stacking merge to generate a focused image. The obtained brightfield, darkfield and fluorescence images are directly shown in the results. Furthermore, the darkfield images are used for particle analysis, which will be described in the following subsection.

A total of 3 images per mode (brightfield or fluorescence) and binder were recorded. Since darkfield microscopy is used for quantification, three different spots per sample were recorded, yielding nine darkfield images per binder, which are later used for particle analysis.

2.3.3. Confocal Laser Scanning Microscope (CLSM)

In this study, a Keyence VK-X1000 CLSM equipped with a VK-D1 motorised XY-stage was employed. Confocal images were recorded with a laser at a wavelength of 661 nm, whereas brightfield optical and topographical images were also recorded. Previous studies have shown that CLSM can depict similar information to AFM with regard to the bee metrics (Pipintakos, 2021a). On the other hand, correlations between the optical CLSM images and brightfield microscopy exist. Therefore, optical CLSM and topographical images are presented in this study. Different magnification levels (from x140 (28 × 5) to x16800 (4 * 28 * 150) of a Nikon Plan Apo EPI objective lens were used for the image processing at a lateral resolution of 5 nm and an axial resolution of 10 nm and numerical aperture between 0.8 and 0.95. Three received images were later used to determine the bee percentage for each binder. All the CLSM images shown in this work were chosen to be depicted in the field of view around 40 × 40 μm in order to facilitate the comparison between the scale of all microscopic images.

2.3.4. Atomic Force Microscope (AFM)

The third microscope used in this study was an Asylum Research MFP-ED AFM in tapping mode. A resonance frequency 300 kHz and spring constant 26 Nm^{-1} of an AC 160 TS cantilever tip were utilised for this study. Concerning the instrumental settings, the vertical Z-axis displacement of the measuring head is constrained to 15 μm, while the sensor noise is less than 25 nm with an average deviation in a 0.1–1 kHz bandwidth for this device. In order to scan the bitumen surface, X and Y activators are used with a travel distance limited to 90 μm, with sensor noise in these directions less than 0.5 nm as an average deviation in a 0.1–10 kHz bandwidth. Based on the interaction between the sample and the tiny probe, at least three topographical images at different scan sizes (from 20 ×20 μm to 80 ×80 μm) were acquired at room temperature and used for the image processing, whereas images of around 40 × 40 μm are shown in this work for the convenience of the reader to compare the different techniques.

2.4. Image analysis

Since the quantification of bitumen microstructure is difficult, two different approaches are employed in this study. First off, particle analysis of optical images is deployed based on previous literature (Mirwald et al., 2020a). However, the previous work focused on evaluating fluorescence images, which is disadvantageous due to similarities in the colour of the fluorescence image (the entire image consists of different shades of green). Furthermore, it should be noted that the samples investigated were prepared by a different preparation procedure (which resemble interface, not surface). Thus, merely the software used (ImageJ Fiji) was adapted and further optimised. The optimisation includes the usage of darkfield images, which will reveal that the bee structures observed on the surface does in fact show light scattering properties. This makes them clearly separable from the rest of the material, allowing a good differentiation between the bee structure and the matrix.

The second approach used evaluates the CLSM and AFM image in regard to the bee identification, which is mainly based on differences in height and depth thresholds. For this approach, one open-source image editing software package (Gwyddion, version 2.58 (Nečas and Klapetek, 2012)) and the accompanying software of the CLSM (VK Multi-FileAnalyzer, version 2.2.0.93) are used for AFM and CLSM respectively. The image processing is based on a 90–95% height or depth threshold, using the height differences between the valleys and peaks of the bee structures and the rest of the bituminous surface.

To compare the different approaches and the microscopes used, the bee percentage was considered the optimum metric as it is a scale-free

and useful value to characterise the observed microstructures.

2.4.1. Particle analysis of darkfield images

The resulting 9 darkfield images shown on the left side of Fig. 2 were used for particle analysis in ImageJ Fiji. A standard threshold selection is enabled, marking all the light scattering bee structures in red (see right side of Fig. 2) while leaving the rest of the matrix unmarked.

The resulting red area is subjected to particle analysis which reveals the number and area of the marked bee structures. Since the bee structures can appear as separate particles in the image, an overall percentage area covered by bee structures (red area) will be shown in the results as particle size and number will not be sufficient. Furthermore, the percentage area covered by bee structures makes such a quantification approach universal to the image size which will be beneficial for comparison to other microscopic techniques. Since 9 images are selected per binder, a good representation of the binder's microstructure is given.

2.4.2. Percentage area of AFM and CLSM images

For the CLSM images, all images were eventually modified on a similar scale for the convenience of the reader and the bee percentage was extracted as the average of three topographical images. Similar height and valley thresholds were imposed on the images after a surface shape correction to exclude any curvature effects due to the inability to obtain completely flat samples. Thus, the peaks and valleys of the bee structures can be isolated from the rest of the image and the total of these areas divided by the image size each time can reveal the bee percentage. It should be noted that any artefacts captured from the suggested analysis are excluded from the bee area.

An example of the peak area identification for AFM is provided in Fig. 3. To facilitate the comparison between the different microscopes, representative images of similar scales are given in Fig. 5–9.

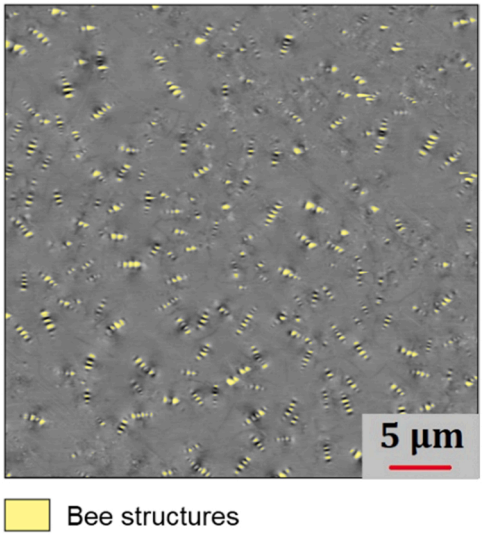

Fig. 3. Indicative image analysis of AFM for the identification of the peak areas of the bee structures.

3. Results

3.1. FTIR

FTIR spectroscopy has been widely used in the asphalt industry to fingerprint bituminous materials. It is a suitable technique to differentiate binders in different modifications or ageing states. However, in the case of identifying other molecular structures, FTIR spectroscopy has its limitations. While the work by Weigel and Stephan, (2018) indicates that FTIR can differentiate refinery, its practical implementation requires complex data analysis and its universal applicability is not yet tested. Even when differences can be observed, no clear indicator to which refinery process has been used can be given. Thus, an FTIR spectrum cannot yet be used to identify this issue. Furthermore, an overall low differentiation in the raw data can be given by the similar availability of functional groups within the material. This is displayed in the resulting spectra in Fig. 4. Looking closer at the fingerprint region in the range of 1800 – 680 cm^{-1}, merely binder B exhibits a significant difference in terms of bands appearing, as a strong band is arising at 1700 cm^{-1}. This can be assigned to the presence of naphthenic acids, which can be found in certain crude oil sources. Another minor difference can be seen at the C=C bands located at 1600, 860, 810 and 750 cm^{-1} as well as differences in the ratio of the CH_2/CH_3 bands located at 2920, 2850,1455, 1375 and 720 cm^{-1}. While these overall minor differences in band intensities indicate a slight discrepancy in binder chemistry, no clear assignment for a specific crude oil source or refinery process can be made yet.Fig. 4).

3.2. Microscopy

In order to give a comprehensive overview of the microstructures captured with the three different microscopes, a total of 6 images per binder will be displayed in the results. The top row consists of the OIM brightfield (left), darkfield (middle) and fluorescence image (right). The bottom row shows the CLSM brightfield (left), topography (middle) and AFM topography images. It should be noted that all three OIM images

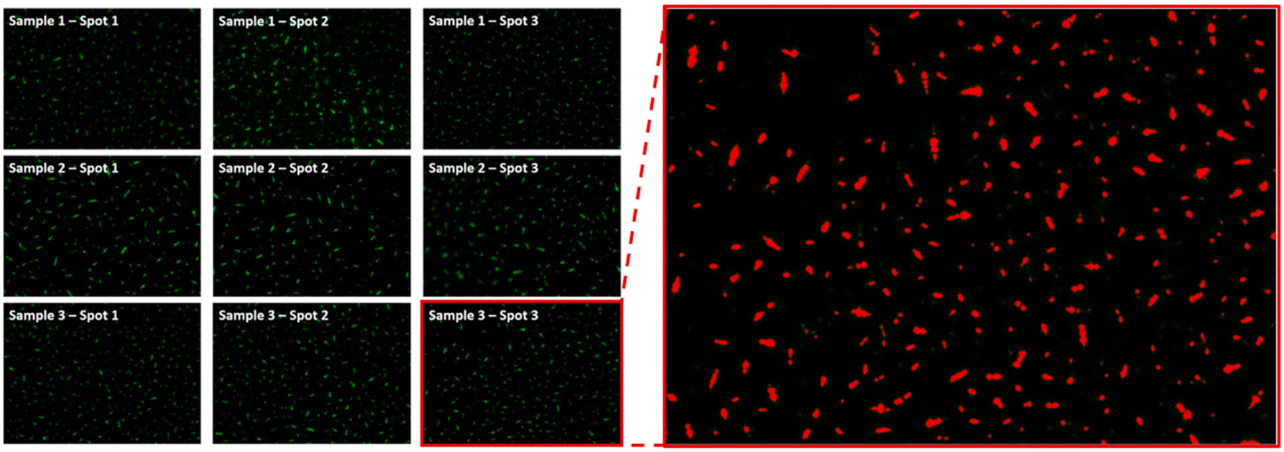

Fig. 2. Overview of the nine darkfield images of a binder (left) and an exemplary result after particle analysis (right).

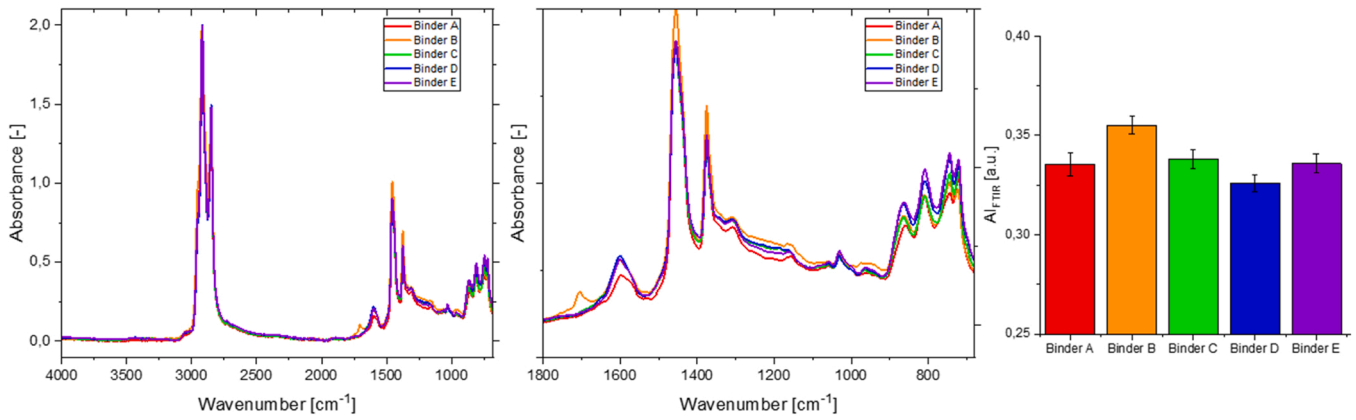

Fig. 4. FTIR spectra of all five binders (left and middle) and the resulting ageing indices (right).

were recorded at the exact same spot at an image size of 50 × 50 μm while different spots were captured with the CLSM and AFM images at an image size range of 20 × 20–80 × 80 μm. Post-process cropping of the AFM and CLSM images was performed to bring the size to a common scale of 40 × 40 μm range. Thus, a slight difference in actual specimen location, and image scale need to be considered.

3.2.1. *Binder A*

Fig. 5 shows the microscopic images of binder A, a straight distilled binder (waxy crude), captured with the OIM, CSLM and AFM. The two left images represent the brightfield images in the OIM (top) and CLSM (bottom), where similar microstructural features can be seen independent of device. Small dark areas appear, which can be associated with the bee structures, as darkfield, CLSM and AFM will reveal. Their blurriness could be explained by the fact that optical devices cannot sharply resolve these microstructural features as they are limited by the Abbe limit and thus resolution. However, it appears that each bee structure is enclosed by a surrounding domain, which is usually referred to as the peri phase (Masson et al., 2006). The brightfield image in the OIM seems to capture this peri phase better than the brightfield image of the CLSM, which could be explained by a difference in the objectives, exposure times and their numerical aperture. The darkfield image (top middle), which only detects light scattering objects, shows the bee structure clearly. This confirms that the bee structures exhibit different physical (optical) properties than the rest of the material and become visible in darkfield. A good similarity can be detected by linking this to both topography images of the CLSM and AFM, which also depict the bee structure nicely. Later imaging analysis (area covered by the bee

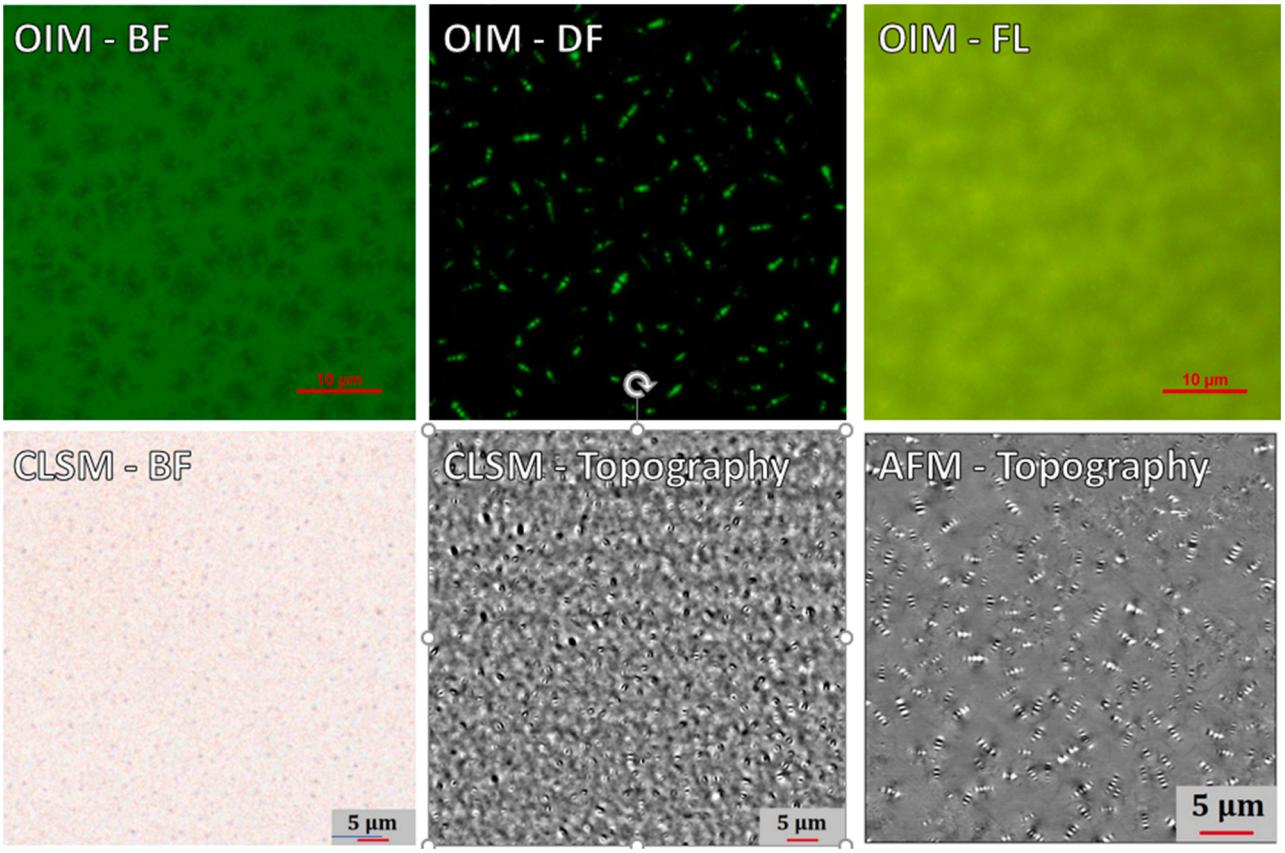

Fig. 5. Microscopic images of binder A in the optical microscope (top) and AFM and CLSM (bottom).

structure) will show whether the particle area detected by darkfield microscopy reflects the coverage of the CLSM and AFM. This could reveal whether these techniques can be linked easily to each other or whether special factors need to be considered regarding the difference in their working principles. The last of the six images, the fluorescence image, is depicted in the top right corner in Fig. 5. Here, an interesting addition to the overall picture can be made, as the peri phase around the bee structures shows a higher fluorescence signal than the rest of the sample surface. Since the fluorescence excitation filter applied is in the range 350 – 450 nm, merely a rough ring-size estimation of 3 – 5 + can be made when the following literature from the early 90 s by Buisine et al., (1993). Furthermore, it remains unclear whether the bee structure itself exhibits the same or lower fluorescence signal compared to the peri phase, as the overall signal detected in the OIM is rather high, which results in a broad fluorescence glow. This glowing could be reduced by application of a confocal fluorescence microscope, which would reduce the surrounding scattering light significantly. This would also increase the sharpness of the fluorescence images.

Overall, the straight distilled binder shows a clear development of the bee structure, which is almost detectable in brightfield images, but strongly pronounced in darkfield, the topography in the CLSM and AFM. The brightfield image in the OIM shows a development of a peri phase, which exhibits a high fluorescence signal in the excitation range of 350 – 450 nm, as displayed by the fluorescence image.

3.2.2. Binder B

The microscopic images of binder B are shown in Fig. 6. This binder is the only binder that does not develop any surface microstructure. Thus, nothing can be seen in the brightfield, topography and the fluorescence images. Surprisingly, not even the darkfield image shows any presence of light scattering particles at or close to the surface. The reason behind the featureless surface of binder B may be found in the refinery process, since this is a pure straight distilled binder. As such, no additional wax formation, typically generated during visbreaking, occurs contrary to i.e. binder C, D or E. On the other hand, since this binder shows the highest amount of FTIR ageing index this may be accompanied by the increase of the polar fractions i.e. high asphaltene content in bitumen. At this stage of the investigations, the debate of the origin of the bee structures is preferred to be kept out of the scope of this study. As this binder does not exhibit any value for the particle analysis, no further microstructural evaluation was performed.

3.2.3. Binder C

Fig. 7 depicts the microstructure of binder C, a visbroken binder. Comparing both brightfield images on the left side, good similarities between OIM and CLSM can be seen. The bee structure is in the centre of a pronounced peri phase, which covers almost the entire surface, compared to the much lower coverage in binder A. However, the bee structure is also observable in the OIM brightfield image. The darkfield image as well as the topography in the CLSM and AFM show the bee structures again. Compared to binder A, the bee structures in the visbroken binder appear larger than that in binder A. Looking at the fluorescence image, again, a brighter signal for the peri phase is observable. However, here one can clearly see that the bee structure in the center of the peri phase does not show significant glowing. Merely various distinct particles exhibit a higher fluorescence, which cannot be associated or linked to the bee structure since they also occur in random locations throughout the material. No clear indication can be made as to what these brightly fluorescing particles can be associated with.

Overall, differences between the different crude oil sources and refinery procedures can be detected. Apparent differences in the peri phase and bee structure size are observable. Later particle area coverage will show whether notable differences between the techniques or samples can be detected.

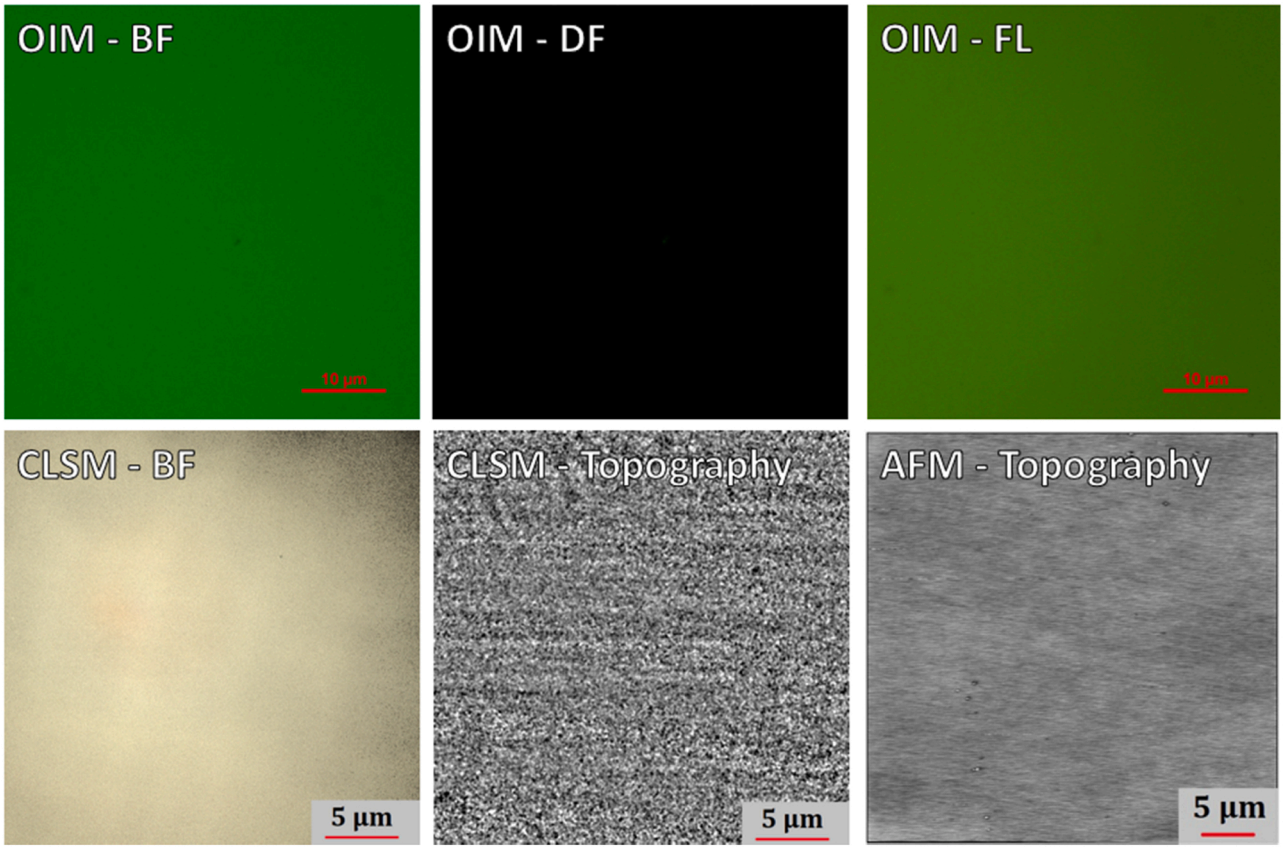

Fig. 6. Microscopic images of binder B in the optical microscope (top) and AFM and CLSM (bottom).

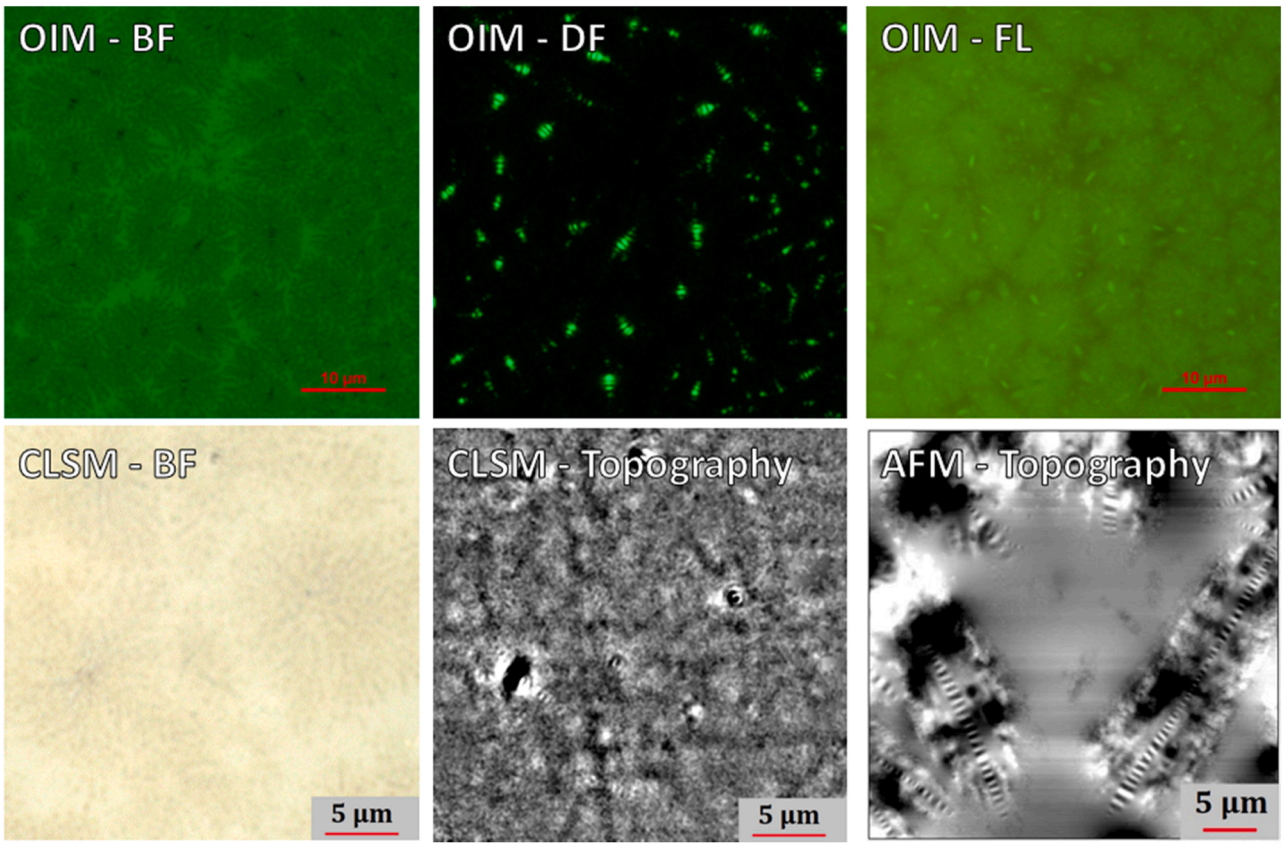

Fig. 7. Microscopic images of binder C in the optical microscope (top) and AFM and CLSM (bottom).

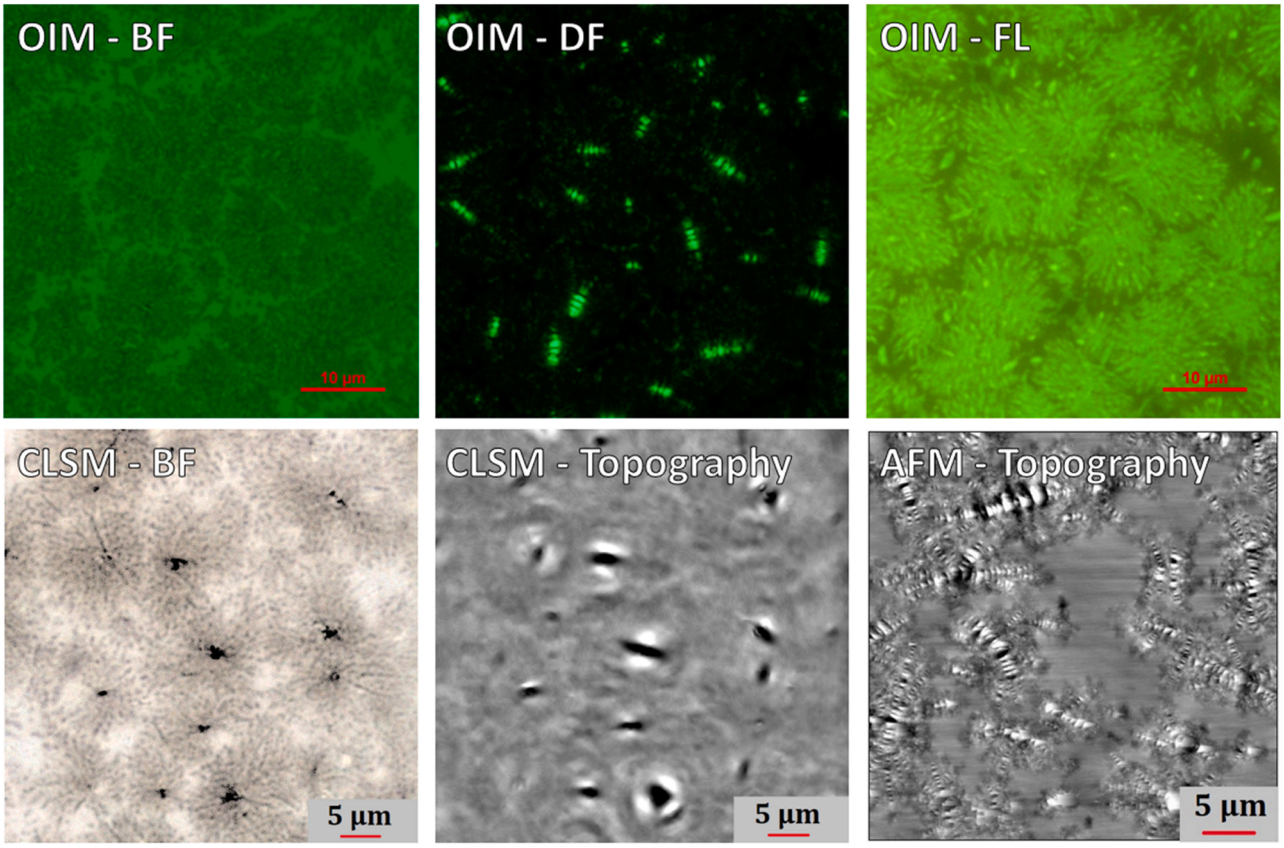

Fig. 8. Microscopic images of binder D in the optical microscope (top) and AFM and CLSM (bottom).

3.2.4. Binder D

Fig. 8 shows the microstructures of binder D, another visbroken binder. This time, the brightfield image of the CLSM displays the bee structures clearly, while the OIM brightfield image merely displays a well-established peri phase. This highlights that standard brightfield microscopy should not be used to test whether a binder develops bee structures or not. However, the darkfield image of the OIM confirms the presence of the bee structures. Similar to other binders, AFM and CLSM topography show the presence of the bee structure. Differences in their percentage area covered will be tackled on later.

Taking a closer look at the darkfield image in the top middle of Fig. 8, a yet unseen observation can be made. While the previous binders (if they developed microstructure) showed a glowing bee structure, this binder also enlightens parts of the peri phase. This indicates that even the peri phase can exhibit light scattering properties. Since all binders were recorded with the exact same illumination parameters, this phenomenon can be assigned to the crude oil or refinery process.

The last of the six images is the fluorescence image in the OIM. Here, a significantly higher fluorescence response (brighter glowing) can be observed, even though the same settings and post-process treatment were applied. This could indicate that the peri phase contains more fluorescing molecules responsible for the signal (e.g. aromatic systems with a size of 3 – 5 + rings). A comparison of binder D and C in fluorescence spectroscopy (Mirwald et al., 2020a) could be performed to justify this hypothesis. Nonetheless, similar to binder C, the peri phase shows a strong signal but no indication that the bee structure itself exhibits any fluorescence capability is provided. Again, small particles with the highest fluorescence signal appear randomly allocated across the sample surface. A separation of the binders into the SARA fractions and re-blending could answer which molecules are responsible for this behaviour.

3.2.5. Binder E

The microstructure of the last of the binders, binder E, is depicted in Fig. 9. Again, similar to the other visbroken binders a peri-phase in the brightfield images is observable. However, it seems to be a mixture between the visbroken binders (C and D) and the straight distilled (A), where even smaller peri phase domains were observed. The darkfield image and topography in the CLSM and AFM show again bee structures. Compared to binder C and D they appear to be much smaller but slightly larger than the ones in binder A. This also fits the observations from the peri phase. Furthermore, similar to binder D, parts of the peri phase possess light scattering properties and show a similar fluorescence behaviour.

3.3. Discussion and comparison of different microscopic techniques

In order to compare and judge the images obtained from the different microscopic techniques a flashback to the working principles is necessary. Starting off with the most used technique in the field of bitumen research, the AFM. The working principles involve a tiny tip in the nanoscale that is attached to a small cantilever. While scanning or tapping across the surface, the cantilever is bending. This bending is detected by a laser diode and a photo detector which then generates the image. The CLSM uses a laser and lenses to illuminate the sample surface and collects the reflected signal with a camera. The sharp contrast is given by the pinhole which eliminates background signals and provides a sharp image from the focal plane of the sample. The working principle of an OIM is similar to the CSLM as light and lenses are used to resolve the microstructure of a sample. However, an OIM does not have a pin hole, which results in a broader signal detected by the camera. This can be seen in the images of the different working modes shown above.

Relating the working principle to the bitumen microstructure it can be concluded that the images observed in the AFM, CLSM and OIM

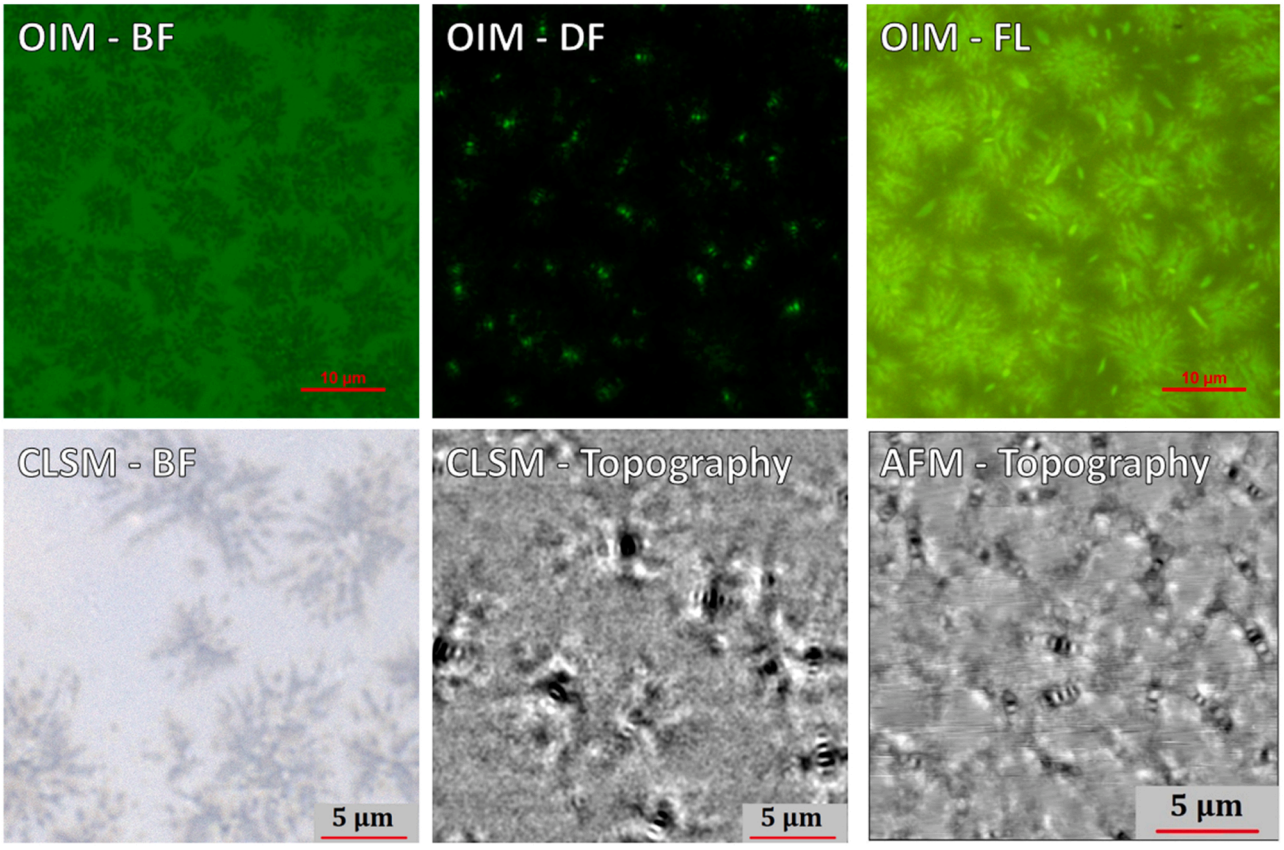

Fig. 9. Microscopic images of binder E in the optical microscope (top) and AFM and CLSM (bottom).

darkfield correspond to different physical properties (AFM: tapping, CLSM: reflected light and OIM darkfield: scattered light). Nonetheless, all three techniques can detect and resolve the bee structure nicely, independent of their working principle. However, when recording the topography, they fail to capture or depict the surrounded peri phase, which was detected mainly by brightfield and fluorescence. While the AFM (Masson et al., 2006) and possibly CLSM could be able to resolve the peri phase, darkfield will only be able to do so, if it exhibits light scattering properties (see binder D and E). On the other hand, brightfield and fluorescence are good candidates to resolve the peri phase around the bee structures, as they fail to resolve the bees most of the time, which could be assigned to their resolution limit. This becomes especially interesting, as the peri phase exhibits a strong fluorescence, which is not yet fully understood.

Thus, researchers can utilise these different techniques to tackle and solve different questions. Future research on the bee structure will most likely include either AFM, CLSM or OIM darkfield, while fluorescence in combination with brightfield can be used to investigate the mystery of the fluorescence of bitumen and how it contributes to the bitumen microstructure.

3.4. Discussion and comparison of the binder microstructure quantification

While the previously shown images display the diversity of bitumen and highlight the similarities and differences between various methods, techniques, crude oil sources and refinery procedures, an approach for quantification of such a microstructure was deemed necessary. Thus, particle or bee structure analysis was carried out from the darkfield, CLSM and AFM images, which are shown in Fig. 10, as they all had a common feature: the bee structure. The respective trends in the area covered by bee structures are given in percent, making it independent of the image size.

Starting with the results of binder A, a similar overall area covered by the bee structure can be seen. While AFM and CLSM, which both detect the material's surface, show values around 3.6%, the darkfield image value of 4.3% is slightly higher. Considering the standard deviations, all three bee structure evaluation results are in a close range to each other. Possible differences could be assigned to threshold definition differences (since darkfield analysis was performed in one laboratory and the AFM and CLSM analysis in the other). As mentioned earlier, this threshold definition is based on a personal selection and not yet universal, as they depend on the image recording parameters. Another possible explanation could be the broadening of the signal in darkfield due to the light scattering of the particle. This could lead to an increased particle size detected by the camera, compared to the images received in the CLSM and AFM. However, this can again be reduced by the threshold selection. No particle or microstructure analysis was conducted for binder B, since it did not develop any detectable microstructure.

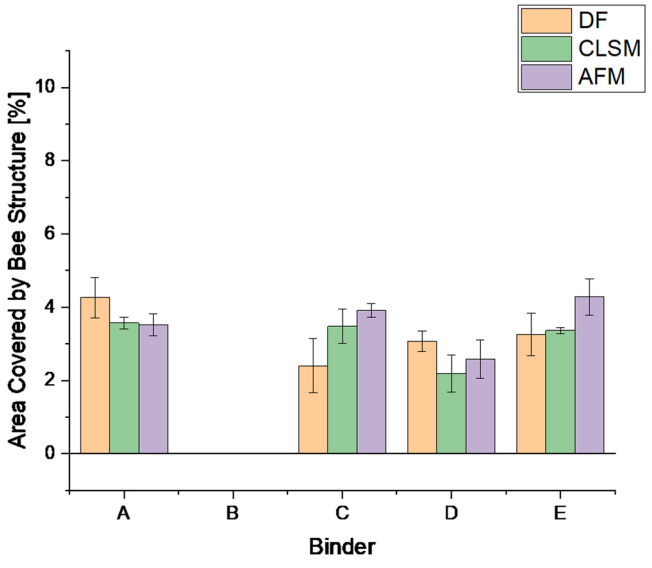

Fig. 10. Results from the area covered by bee structure analysis from darkfield (DF) and topography of CLSM and AFM.

Binder C shows an inverse trend with darkfield (2.4%) being below CLSM (3.5%) and AFM (3.9%). The large standard deviation shows that binder C's homogeneity varied significantly.

An extreme example is given in Fig. 11, where two spots on the different specimens from binder C show a drastic difference in the bee structure occurrence and size. This highlights the complexity of the material and the diversity within one sample. Even when following a strict sample preparation technique, significant differences in the surface microstructure can be detected. Whether any special post preparation treatment or relaxation could reduce this scattering remains unanswered. However, it needs to be kept in mind that the material's surface can age and change very rapidly, which can bias the results caused by any further heating or heat treatment. Thus, some middle ground, considering these factors should be selected.

For binder D, a similar trend then for binder A can be seen with the darkfield (3.1%) being above CLSM (2.2%) and AFM (2.6%). The values of binder E are a bit higher compared to binder D, with darkfield being the lowest at 3.3%, followed by CLSM at 3.4% and AFM at 3.9%.

Overall, the standard deviations of all three techniques show an overlap for all samples, which indicates a close proximity for the values and a sufficiently close connection between the three techniques and their respective microstructural evaluation. However, no clear differentiation or separation into crude oil source or refinement process (visbreaking or straight distilled) can be detected via this area covered by bee structure parameter. When looking at the images from Fig. 5–9, a large diversity in the microstructures can be seen. Thus, it is worth looking into other parameters like the bee structure size, shape or orientation in the future. Furthermore, it should be noted that in order to obtain a representative result, a large image pool or area per binder surface should be considered. Thus, this study recommends using around 9 images per binder to obtain a sufficient statistical significance for judging the quantification of a binder's microstructure in the future.

4. Conclusion

This study used three different microscopes, OIM, CLSM and AFM, to investigate five unmodified bituminous binders originating from different crude oil sources and refineries. Two of the binders were straight distilled binders, while the rest were visbroken binders. An initial comparison of FTIR spectroscopic data revealed that no clear differentiation between the binders can be made. Merely one binder exhibits a carbonyl band in the original state. Thus, to overcome this issue, different microscopic techniques and working modes were applied, including the application of brightfield (CLSM, OIM), darkfield (OIM), fluorescence (OIM) and topography (AFM, CLSM).

The three visbroken binders developed bee structures surrounded by a prominent peri phase. These bee structures were always observable in AFM, CLSM and darkfield microscopy. Brightfield nicely illustrated the surrounding peri phase, which exhibits a strong fluorescence.

One of the straight distilled binders developed no microstructure, while the other straight distilled binder developed smaller bee structures surrounded by a smaller peri phase.

Performing particle or microstructural analysis of darkfield, CLSM and AFM topography images, the area covered by bee structures could be determined. All three microscopic techniquies yielded similar values with overlapping standard deviations for those binders that developed a microstructure. However, the overall values ranged between 2.4% and 4.3%, with relatively large standard error bars. Thus, no clear differentiation between binders could be accessed via the area covered by bee

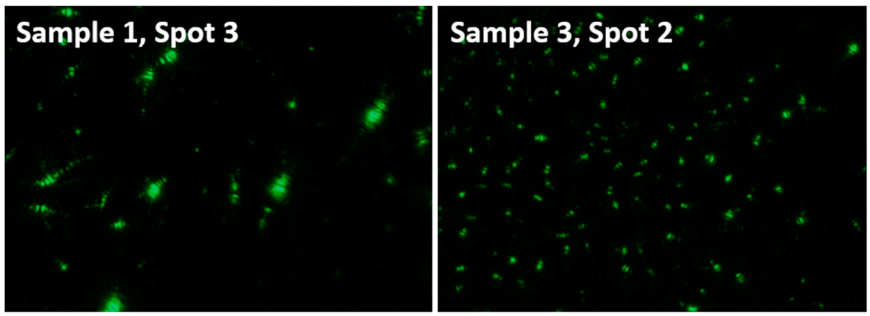

Fig. 11. Comparison of two darkfield images from binder C.

structures. Nonetheless, by visual consideration, this study showed how different binders can behave in microscopy and how each of the presented techniques can be used and compared. Future work will focus on further optimisation of the microstructure evaluation. This can be used to differentiate binders and to quantify bitumen microstructure and tackle questions related to how the microstrucutre is affected by storage time and thermal history. Such work will include a larger sample pool and image number (9 images per binder), which should provide sufficient data for statistical significance. Furthermore, this work can be used as a basis for tackling relevant questions on how ageing changes the microstructure of bitumen and how significant these changes need to be in order to be detected via microstructural analysis.

Funding

The authors would like to thank Lukas Eberhardsteiner for providing access to the OIM microscope at the TU Wien. The financial support by the Austrian Federal Ministry for Digital and Economic Affairs, the National Foundation for Research, Technology and Development and the Christian Doppler Research Association is gratefully acknowledged. Furthermore, the authors would also like to express their gratitude to the CD laboratories company partners BMI Group, OMV Downstream and Pittel+Brausewetter for their financial support as well as the University of Antwerp for funding the AQ^{2}UABIT (project no. 40204) and the FWO/WOG project (project no. 46958).

Declaration of Competing Interest

The authors declare the following financial interests/personal relationships which may be considered as potential competing interests. Johannes Mirwald reports financial support was provided by Christian Doppler Research Association.

ReferenceS

Aguiar-Moya, J.P., et al., 2015. Morphological analysis of bitumen phases using atomic force microscopy. Road Mater. Pavement Des. 16 (sup1), 138–152.
Aguiar-Moya, J.P., et al., 2017. Effect of ageing on micromechanical properties of bitumen by means of atomic force microscopy. Road Mater. Pavement Des. 18 (sup2), 203–215.
Bearsley, S., Forbes, A., Haverkamp, R.G., 2004. Direct observation of the asphaltene structure in paving-grade bitumen using confocal laser-scanning microscopy. J. Microsc. 215 (Pt 2), 149–155.
Blom, J., et al., 2021. New evidence on the origin of 'bee structures' on bitumen and oils, by atomic force microscopy (AFM) and confocal laser scanning microscopy (CLSM). Fuel 303, 121265.
Buisine G., J.M.J., Such, C., Farcas, F., Ramond, G., Claudy, P., Létoffé, J.M., King, G.N., Planche, J.P., Germanaud, L., 1993. Thermodynamic behavior and physicochemical analysis of eight SHRP bitumens. Transp. Res. Rec. (1386), 1–9.
Handle, F., 2016. The bitumen microstructure: a fluorescent approach. Mater. Struct. 49 (1–2), 167–180.
Hasheminejad, N., 2021. Utilizing deep learning and advanced image processing techniques to investigate the microstructure of a waxy bitumen. Constr. Build. Mater. 313, 125481.
Hofko, B., et al., 2016. Impact of maltene and asphaltene fraction on mechanical behavior and microstructure of bitumen. Mater. Struct. 49 (3), 829–841.
Jing, R., 2019. Ageing effect on chemo-mechanics of bitumen. Road Mater. Pavement Des. 1–16.
Loeber, L., 1996. New direct observations of asphalts and asphalt binders by scanning electron microscopy and atomic force microscopy. J. Microsc. Oxf. 182, 32–39.
Lu, X., 2005. Wax morphology in bitumen. J. Mater. Sci. 40 (8), 1893–1900.
Lu, X.H., et al., 2018. Microstructures of bitumen observed by environmental scanning electron microscopy (ESEM) and chemical analysis using time-of-flight secondary ion mass spectrometry (TOF-SIMS). Fuel 229, 198–208.
Masson, J.F., Leblond, V., Margeson, J., 2006. Bitumen morphologies by phase-detection atomic force microscopy. J. Microsc. 221, 17–29.
Mikhailenko, P., Kadhim, H., Baaj, H., 2017. Observation of bitumen microstructure oxidation and blending with ESEM. Road Mater. Pavement Des. 18, 216–225.
Mirwald, J., et al., 2020b. Impact of reactive oxygen species on bitumen aging – the Viennese binder aging method. Constr. Build. Mater. 257, 119495.
Mirwald, J., et al., 2022b. Impact of UV–Vis light on the oxidation of bitumen in correlation to solar spectral irradiance data. Constr. Build. Mater. 316, 125816.
Mirwald, J., Hofko, B., Grothe, H., 2020a. Utilising fluorescence spectroscopy and optical microscopy to investigate bitumen long-term ageing. Road Mater. Pavement Des. 1–14.
Mirwald, J., Nura, D., Hofko, B., 2022a. Recommendations for handling bitumen prior to FTIR spectroscopy. Mater. Struct. 55 (2), 26.
Nahar, S.N., 2013. Temperature and thermal history dependence of the microstructure in bituminous materials. Eur. Polym. J. 49 (8), 1964–1974.
Nečas, D., Klapetek, P., 2012. Gwyddion: an open-source software for SPM data analysis. Open Phys. 10 (1), 181–188.
Pipintakos, G., et al., 2021a. Coupling AFM and CLSM to investigate the effect of ageing on the bee structures of bitumen. Micron 151, 103149.
Pipintakos, G., et al., 2021b. Application of atomic force (AFM), environmental scanning electron (ESEM) and confocal laser scanning microscopy (CLSM) in bitumen: a review of the ageing effect. Micron 147, 103083.
Poulikakos, L.D., et al., 2019. Impact of asphalt aging temperature on chemo-mechanics. RSC Adv. 9 (21), 11602–11613.
Ramm, A., 2016. Optical characterization of temperature- and composition-dependent microstructure in asphalt binders. J. Microsc. 262 (3), 216–225.
Ramm, A., et al., 2019. Morphology and kinetics of asphalt binder microstructure at gas, liquid and solid interfaces. J. Microsc. 276 (3), 109–117.
Rozeveld, S.J., 1997. Network morphology of straight and polymer modified asphalt cements. Microsc. Res Tech. 38 (5), 529–543.
Stangl, K., Jäger, A., Lackner, R., 2006. Microstructure-based identification of bitumen performance. Road Mater. Pavement Des. 7 (sup1), 111–142.
Weigel, S., Stephan, D., 2018. Differentiation of bitumen according to the refinery and ageing state based on FTIR spectroscopy and multivariate analysis methods. Mater. Struct. 51 (5), 1–11.